npj climate and atmospheric science

www.nature.com/npjclimatsci

ARTICLE OPEN

Check for updates

QBO modulation of MJO teleconnections in the North Pacific: impact of preceding MJO phases

Min-Jee Kang[1], Hera Kim[1] and Seok-Woo Son[1]✉

This study examines the influence of the Quasi-Biennial Oscillation (QBO) on the Madden-Julian Oscillation (MJO) teleconnections in the North Pacific using ERA5 data. It is found that the Rossby wave trains induced by MJO phase 6–7 exhibit greater strength and robustness during the westerly QBO winter (WQBO) than during the easterly QBO winter (EQBO), although the MJO itself is weaker during the former. This counter-intuitive dependency of MJO teleconnections on the QBO is attributed to the preexisting MJO teleconnections prior to the MJO phase 6–7. The MJO phase 6–7 is more frequently preceded by stronger MJO phase 3–4 during the EQBO than during the WQBO. The preceding MJO phase 3–4 teleconnections, which have opposed signs to the MJO phase 6–7 teleconnections, result in a considerable attenuation of the MJO phase 6–7 teleconnections by destructive interference. This result is supported by linear model experiments. The subseasonal-to-seasonal prediction models also indicate improved prediction skills of MJO phase 6–7 teleconnections during the WQBO compared to the EQBO. These results suggest that enhanced MJO activities during the EQBO do not necessarily result in stronger and more robust MJO teleconnections in the North Pacific.

npj Climate and Atmospheric Science (2024)7:12 ; https://doi.org/10.1038/s41612-024-00565-w

INTRODUCTION

The Madden-Julian oscillation (MJO) is one of the most prominent intraseasonal oscillations in the tropics. It is characterized by the eastward movement of planetary-scale convection anomalies along the equator from the Indian Ocean to the Western Pacific in 30–90-day period[1,2]. As the MJO excites the Rossby wave trains similar to the Pacific-North America (PNA) pattern that propagates poleward[3,4], it has profound impacts on the midlatitude weather and climate systems[5–7]. In particular, MJO phases 2–3 and 6–7 (hereafter, P23 and P67) are known for their robust teleconnections due to their dipole-structured convection anomalies[8].

Yoo and Son[9] reported that the MJO amplitude is modulated by the quasi-biennial oscillation (QBO) during the boreal winter. The QBO is a dominant interannual oscillation in the tropical stratosphere, showing alternative easterly and westerly winds in the equatorial stratosphere with a mean period of 28 months[10,11]. When the boreal winter QBO is in the easterly phase (EQBO), MJO amplitude is larger, and its occurrence frequency is higher compared to the westerly phase (WQBO)[12]. Son et al.[13] and the subsequent studies[14–18] proposed that the QBO-induced secondary circulation and cloud-radiative feedback could partly account for such differences (see also Martin et al.[19] and references therein).

Since the MJO teleconnections arise from the Rossby wave trains excited by the tropical convection anomalies, one might expect that MJO teleconnections would be stronger with stronger MJO under the EQBO condition compared to the WQBO condition. Indeed, during the EQBO winter, MJO-related 300-hPa streamfunction anomalies are strengthened over the western North Pacific at MJO P23[13] and precipitation anomalies are enhanced over East Asia at MJO P23 and P678[20]. However, several counterexamples have also been suggested. For example, Feng and Lin[21] reported a stronger connection between the MJO and North Atlantic Oscillation (NAO) during the WQBO winter at MJO P3 and P7. They argued that a southward shift of the Asian-Pacific jet associated with the WQBO[22] provides a favorable condition for planetary waves to propagate into the stratosphere. The intensified planetary waves can weaken the stratospheric polar vortex, thereby influencing the NAO[23] via downward coupling. Song and Wu[24] showed stronger 300-hPa streamfunction and sea-level pressure anomalies in the North Pacific during the WQBO winter at MJO P67. This QBO modulation effect was again attributed to the Asian-Pacific jet change. However, it is difficult to attribute strong MJO teleconnections during the WQBO winter solely to the mean-flow change, as MJO teleconnections were known to be stronger only at MJO P67 but not at P23 in the literature[13,24].

The aforementioned studies suggest that the modulation of MJO teleconnections by the QBO varies from one region to another. While MJO teleconnections exhibit stronger intensity during the EQBO winter in East Asia[20], they show stronger intensity during the WQBO winter in the North Atlantic[21]. In the North Pacific region, however, the QBO modulation of MJO teleconnections also appears to depend on the phase of the MJO[13,24]. Such an incoherent feature calls for a systematic investigation of MJO teleconnections during the two QBO states in the North Pacific region.

The lack of clarity also appears in the prediction skill of MJO teleconnections. Contrary to the common expectation that the enhanced MJO predictions during the EQBO winter[25,26] would result in improved midlatitude prediction skills, midlatitude prediction skills are higher during the WQBO winter for specific MJO phases especially around the North Pacific region. For instance, atmospheric river is found to be more predictable during the WQBO winter at lag three weeks of MJO P567 along the west coast of North America[27,28]. By investigating the QBO modulation of the prediction skills of MJO-related circulation variability using a Sensitivity to the Remote Influence of Periodic Events (STRIPES) index[29], Mayer and Barnes[30] found that the prediction skill of STRIPES index, a circulation variability coherent with the full cycle of the MJO, shows no substantial improvement in the North Pacific during the EQBO winter compared to the WQBO winter.

[1]School of Earth and Environmental Sciences, Seoul National University, Seoul, South Korea. ✉email: seokwooson@snu.ac.kr

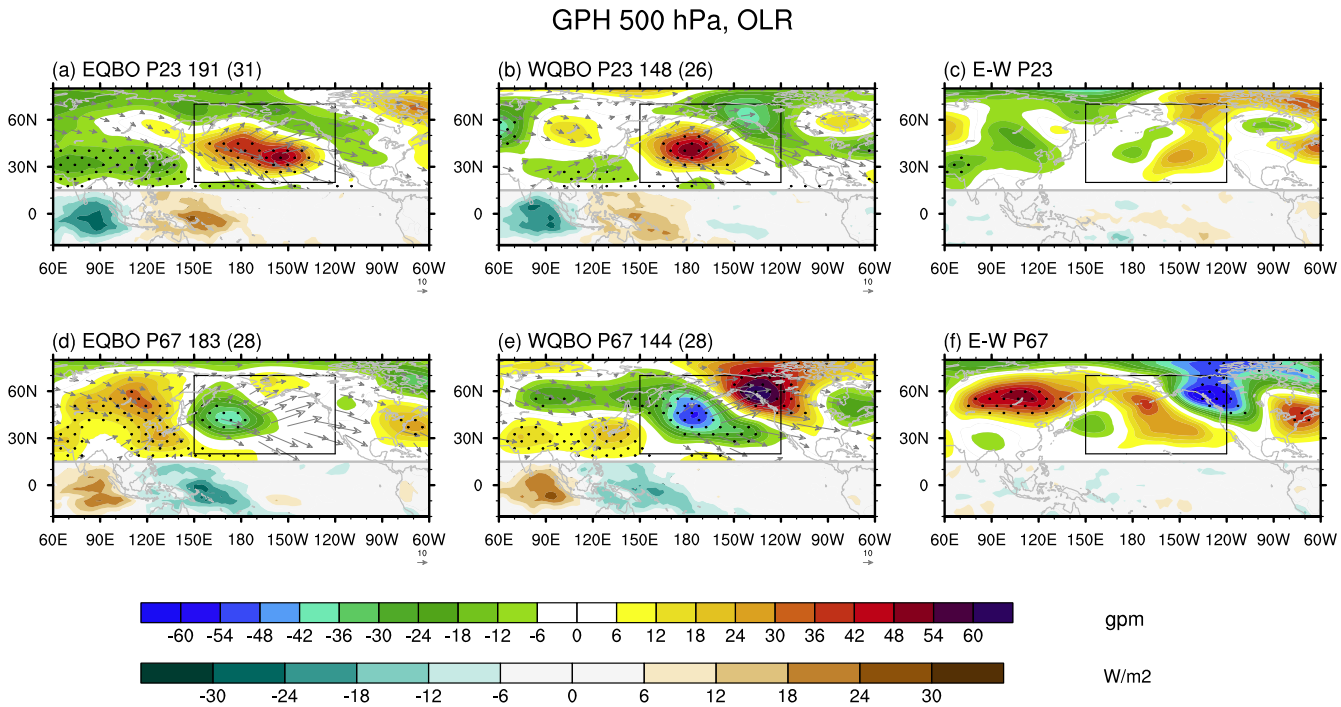

Fig. 1 OLR anomalies at MJO P23 and P67 and their teleconnection during the two QBO winters. (Top) Composite of OLR anomalies for MJO phase 23 event (20°S-15°N) and lagged composite of anomalous geopotential height at 500 hPa for lag 5–10 days after the MJO P23 event (15°-80°N) during **a** EQBO winters, **b** WQBO winters, and **c** the differences between the two. (bottom). **d**–**f** Same as in top panels but for the MJO P67 event. The stippled areas denote the regions where the values are statistically significant at the 95% confidence level. The boxed region indicates where the MJO-teleconnection is strong regardless of the phase, which will be used to diagnose pattern consistency. Gray vectors represent the horizontal component of the stationary Rossby waves. The number in the subtitle of each panel indicates the number of events, and the number inside the parenthesis indicates the number of degrees of freedom.

To better understand the MJO teleconnections and their interannual modulation by the QBO, the present study explores the MJO teleconnections in the North Pacific region during the two QBO winters by using geopotential height at 500-hPa level. Our goal is to specify the MJO phases that exhibit strong and robust teleconnections during the WQBO winter compared to the EQBO winter and to investigate the underlying mechanisms. It turns out that MJO teleconnections in the North Pacific are enhanced and more robust during the WQBO winter when the MJO is at P67. Their enhancement is explained by the fact that MJO P34 prior to P67, which serves to partly cancel the MJO P67 teleconnections, is weaker during the WQBO winter. This argument is supported by a series of linear-model experiments. The implication of the present study on the subseasonal-to-seasonal (S2S) prediction is also discussed.

RESULTS

QBO modulation of MJO teleconnections

Figure 1 illustrates the OLR anomalies and the lagged response of 500-hPa geopotential height anomalies for MJO P23 and P67 during the two QBO winters. Regardless of the QBO phase, MJO-induced Rossby waves propagate northeastward from the subtropical Rossby gyres, having strong anomalies in the North Pacific region (20°–70°N and 150°E-120°W; boxed region in Fig. 1). For MJO P23 (Fig. 1a–c), no significant or systematic differences are observed between the two QBO winters, although there is a slight westward shift in the positive center (30°N, 145°W to 40°N, 180°) and a strengthening of the negative center (70°N, 140°W) during the WQBO winter. Compared to P23, P67 exhibits a strong teleconnection pattern during the WQBO winter, particularly in the North Pacific (Fig. 1d–f). Within the boxed region, the MJO P67 teleconnections during WQBO winter distinctively show an intensified negative-positive dipole, with particular significance observed at the positive center (Fig. 1e, f). Note that the stronger MJO P67 teleconnections during WQBO winters extend beyond the North Pacific to downstream regions, which are likely affected by those in the North Pacific. These results suggest that MJO-teleconnection differences between the two QBO winters are phase-dependent in the North Pacific. Specifically, MJO P67 shows enhanced and more robust teleconnections in the North Pacific during the WQBO winter compared to the EQBO winter, although the MJO itself is weaker and less organized during the WQBO winter.

Figure 2 shows the MJO-teleconnection pattern consistency in the North Pacific region (boxed region in Fig. 1) as a function of MJO phase and days after each MJO event[31]. The pattern consistency is investigated here to quantify the robustness of the teleconnection pattern. During the WQBO winter (Fig. 2b), two distinct regions of high pattern consistency, extending from lag 0 of P34 and P78, are observed. Considering that it takes about one to two weeks for the MJO teleconnections to mature in the North Pacific[8,31], these enhanced pattern consistency bands likely result from the lagged responses of midlatitude circulation to MJO P23 and P67. However, the high pattern consistency bands are not evident during the EQBO winter (Fig. 2a). This result implies that the enhanced pattern consistency in the North Pacific after MJO P23 and P67[31] is confined to during the WQBO winter. As the MJO-teleconnection during the WQBO exhibits a high pattern consistency, the distinct two-striped pattern is also found in the difference between the two QBO winters (Fig. 2c). Note that a statistically significant difference is observed exclusively on the right side of the stripes. This result again suggests that MJO-P67 teleconnections are more consistent and robust when the tropical wind at 50 hPa is westerly than easterly in the boreal winter (Fig. 1f). Given the high consistency of the PNA-like teleconnections in

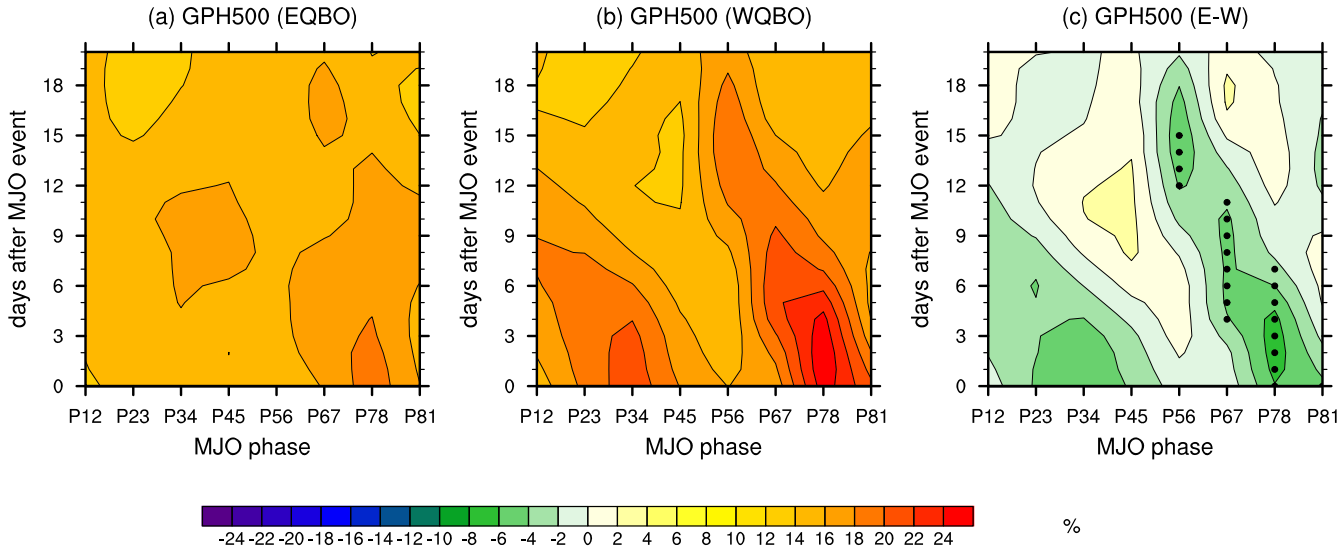

Fig. 2 Pattern consistency of MJO teleconnections during the two QBO winters. The pattern consistency of geopotential height anomalies at 500 hPa as a function of MJO phase and lag day (i.e., days after MJO event) in the North Pacific region (20°–70°N, 150°E–120°W; boxed in Fig. 1) during the **a** EQBO winters and **b** WQBO winters and **c** the differences between the two.

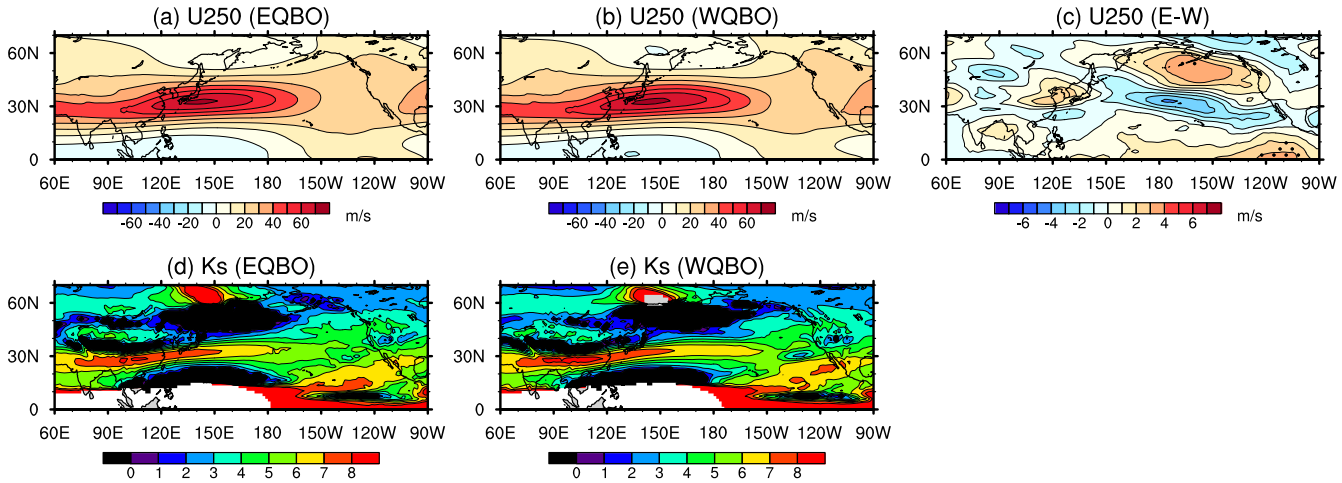

Fig. 3 Zonal wind and stationary wavenumber during the two QBO winters. (Top) DJF-mean zonal wind at 250 hPa during the **a** EQBO winters and **b** WQBO winters, and **c** the differences between the two. Statistically significant differences at the 95% confidence level are stippled. (bottom) DJF-mean stationary Rossby wavenumber K_s during the **d** EQBO winters and **e** WQBO winters.

the North Pacific at MJO P67 during the WQBO winters, all analyses below are focused on MJO P67.

Previous studies postulated that stronger MJO P67 teleconnections during the WQBO winter are attributed to the background-flow change by the QBO. This postulation stems from the fact that the subtropical jet, which acts as a guide for the MJO-induced Rossby waves[32], is displaced southward during the WQBO[22,33,34]. The southward displacement of the jet can provide a favorable condition for the Rossby wave propagation beyond the North Pacific[35]. Figure 3a–c, which illustrate the DJF-mean zonal winds at 250 hPa, indeed exhibit a hint of an equatorward shift of the jet during the WQBO winter in comparison to the EQBO winter. However, the zonal wind differences between the two QBO states do not display any statistical significance (Fig. 3c), which is likely associated with the weak impact of the QBO on the Pacific jet during the midwinter[33,36].

The stationary wavenumber for the Rossby waves $[K_s = (\beta_*/U)^{1/2}$, where $\beta_* = \beta - \partial^2 U/\partial y^2]$[32] shows an eastward extension of the region of high K_s (Fig. 3d, e). It indicates a slight elongation of the waveguide towards the North Pacific during the WQBO winter. However, it cannot fully elucidate why MJO-P67 teleconnections are particularly affected by the QBO in contrast to MJO P23 teleconnections. It instead suggests that other factors beyond the mean-flow change by the QBO contribute to the phase-dependent QBO modulation of MJO teleconnections.

Figure 4a–c depicts Hovmöller diagrams illustrating the 20–100 day filtered outgoing-longwave radiation (OLR) anomalies from lag −25 to +5 days. They are averaged over the equatorial region (10°N–10°S) for MJO P67. Overall, OLR anomalies show eastward propagation over time, thereby OLR anomalies at lag −10 day or earlier display nearly opposite signs to those at lag 0 (Fig. 4a, b). When examining the difference between the EQBO and WQBO winters (Fig. 4c), a notable difference is found at lag −10 day or earlier, at which the OLR anomalies exhibit significantly greater intensity during the EQBO winter. The zonal structure is also more distinct during the EQBO winter (compare Fig. 4a, b), suggesting that it is likely better projected onto the canonical MJO structure. It makes a stronger MJO amplitude from lag 0 back to lag −20 days during the EQBO winter compared to the WQBO winter (cf. Fig. 5).

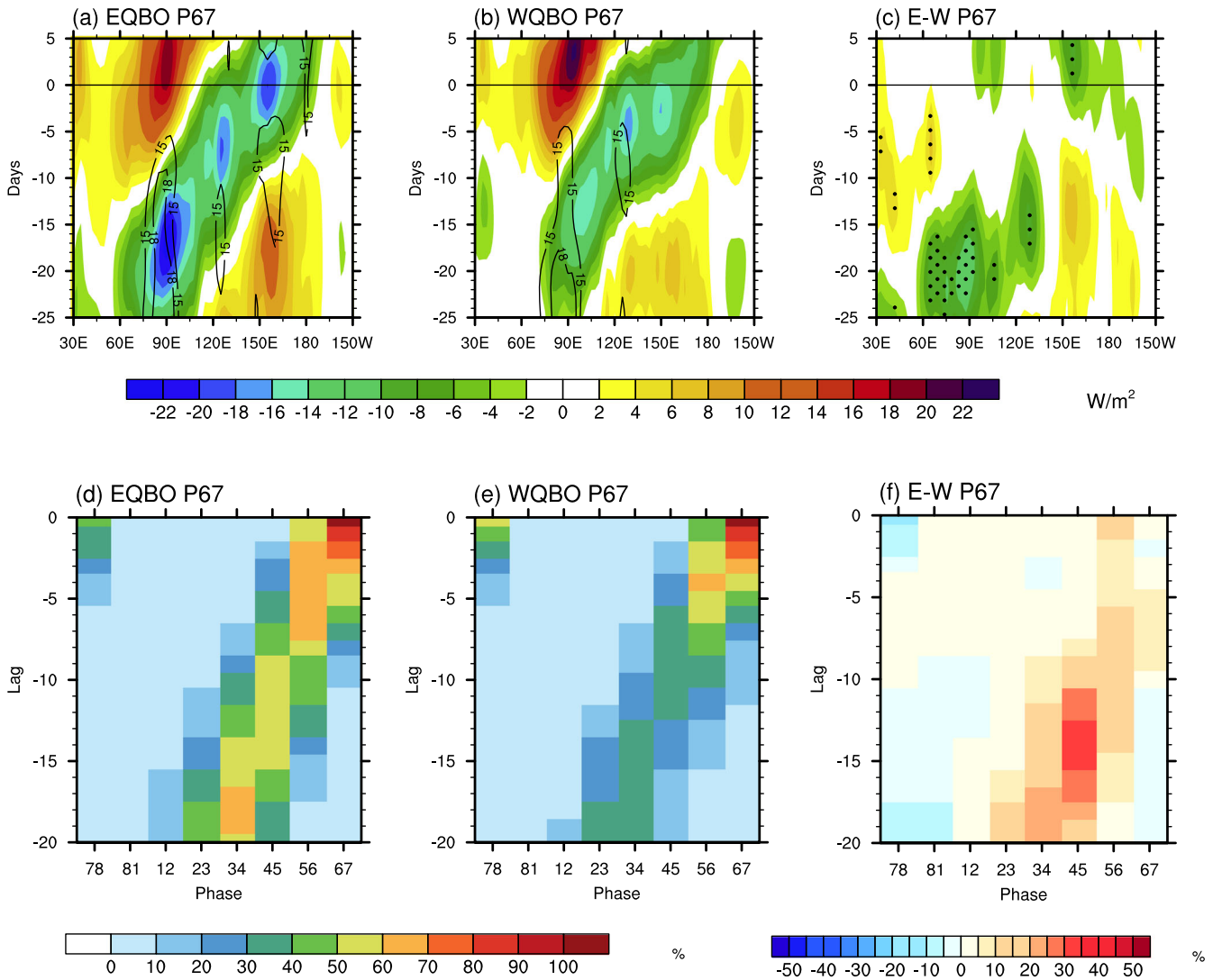

Fig. 4 Hovmöller diagram of OLR anomalies and back trajectory of MJO P67 during the two QBO winters. (Top) Hovmöller diagram of OLR anomalies (20–100 day filtered) averaged over the equatorial region (10°N–10°S) during the MJO P67, from lag −25 to lag 5, for the **a** EQBO winters, **b** WQBO winters, and **c** the differences between the two (shading). The contour denotes the standard deviation across MJO events (15, 18, and 21 W/m^2). Statistically significant differences at the 95% confidence level are stippled. (bottom) The number of MJO events from lag −20 to lag 0, starting from MJO P67, normalized by the number of MJO P67 during the **d** EQBO winters, **e** WQBO winters, and **f** the differences between the two. Here, lag 0 is defined as all identified MJO P67 days in Fig. 1.

It is notable that at lag −10 day or earlier, the standard deviation of OLR anomalies is smaller during the WQBO winter (contour in Fig. 4a, b). This result suggests that the time-accumulated OLR anomaly pattern or intensity at MJO P67 exhibits less variability across MJO events during the WQBO winter compared to the EQBO winter, potentially leading to the higher pattern consistency in Fig. 1b.

Figure 4d–f illustrate the back trajectory of the MJO, which is retraced from lag 0 of P67 in reverse. To obtain the trajectory, the MJO phase is first recorded from lag 0 to −20 day for each MJO event. Only cases with an OLR-based MJO index (OMI) amplitude greater than or equal to 1 are included. Next, the number of events for each MJO phase and each time lag are counted and subsequently normalized by the total number of MJO events for each MJO phase. This normalization addresses any discrepancies in the number of MJO events between the two QBO states. During the EQBO winter, MJO P67 events are typically traced back to P34 (Fig. 4d), whereas during the WQBO winter, most cases tend to persist at P567 (Fig. 4e). Their difference clearly shows that a greater number of MJO events are recorded at P34 during the EQBO winter compared to during the WQBO winter at time lags of −5 to −20 days (Fig. 4f), consistent with the Hovmöller diagram in Fig. 4a–c. This result indicates that during the WQBO winter, MJO P67 originates from the east of the Maritime Continent (MC) or that it is preceded by a significantly weak opposite-signed MJO phase prior to itself. On the other hand, during the EQBO winter, MJO P67 is preceded by a strong opposite-signed MJO phase with enhanced convection at the west of the MC.

The averaged phase diagram of MJO P67 (Fig. 5) confirms that MJO P34 followed by MJO P67 is substantially weaker during the WQBO winter. Notably, for lag −9 day or earlier, MJO amplitude is smaller than 1 during the WQBO winter, while it remains larger than 1 until lag −20 day during the EQBO winter. This may be because the MC-barrier effect, the difficulty of the MJO to propagate across the MC, is stronger during WQBO winters[16,37]. Since MJO convection over the Indian Ocean at P23 tends to weaken crossing the MC during the WQBO winter, MJO convection of P67 is more likely to originate in the western Pacific.

The above finding raises the question of whether the intensity of the MJO P34 prior to the MJO P67 could have an impact on the

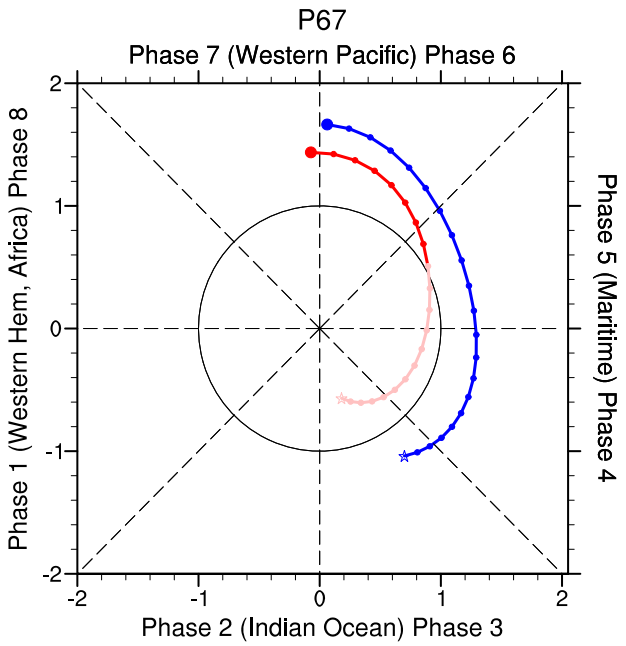

Fig. 5 Phase diagram of MJO P67 during the two QBO winters. Phase diagrams of the composited MJO P67 from lag 0 (circle) to lag −20 (star) during the EQBO winters (blue) and WQBO winters (red), where the composite refers to the averaged MJO phase at a given lag day based on Fig. 4d, e. Light colors represent the composited values with OMI amplitudes smaller than 1.

MJO-P67 teleconnections. Specifically, do the stronger MJO-P67 teleconnections during the WQBO result from the absence (or weakness) of the preceding MJO-P34 teleconnections? The MJO-P34 teleconnections oppose the MJO-P67 teleconnections. If the former is maintained for a few weeks, its presence prior to MJO P67 could weaken the MJO-P67 teleconnections through destructive interferences.

Conceptually, QBO influence on MJO-P67 teleconnections could be categorized into two components. The first one is the amplitude modulation effect, which refers to the QBO's effect on the MJO amplitude[9]. As the MJO amplitude tends to be larger during the EQBO winter, stronger teleconnection is expected during the EQBO winter than during the WQBO winter. The second one is MC barrier modulation effect, indicating less hindrance of MJO propagation across the MC during the EQBO winter. In such case, the presence of MJO P34 that might generate Rossby wave trains destructively interfering with MJO-P67 teleconnections could lead to weak and disorganized MJO-P67 teleconnections in the North Pacific region during the EQBO winter.

The tug-of-war between these two effects, i.e., the amplitude modulation effect versus the MC-barrier modulation effect, likely determines the MJO teleconnections 5–10 days after P67. If the latter is dominant, the teleconnections in the North Pacific can be stronger during the WQBO winter.

Linear model experiments

To verify this hypothesis, a series of linear baroclinic model (LBM) experiments are conducted. Figure 6 shows the experimental setup. For the horizontal distribution (Fig. 6c), idealized MJO forcing mimicking the observed heating is prescribed. For the vertical distribution (Fig. 6b), a simplified vertical profile is utilized. The duration of each MJO phase is set to 5 days[38]. To reproduce the MJO forcing under the EQBO and WQBO conditions, the same structure of forcing as in Fig. 6b, c is used, but for the WQBO experiment the magnitude of the forcing is multiplied by a factor of 0.4 at MJO P34 ($W_{34}/E = 0.4$) and by a factor of 0.9 at MJO P567 ($W_{567}/E = 0.9$) compared to that of the EQBO experiment where the forcing amplitude is set to 1.0 (Fig. 6a). The values of W_{34}/E and W_{567}/E are determined based on the relative amplitude of the observed MJO (cf. Fig. 5). Note that W_{567}/E smaller than 1 represents the amplitude modulation effect (e.g., weak MJO amplitude during the WQBO), while W_{34}/E smaller than W_{567}/E reflects the MC-barrier modulation effect (e.g., weak MJO P34 prior to MJO P567 during the WQBO). After conducting this control experiment, a sensitivity experiment is also performed by sweeping W_{34}/E and W_{567}/E to investigate the tug-of-war between the amplitude modulation effect and the MC-barrier modulation effect.

Figure 7 shows the linear response of 500-hPa geopotential height to the prescribed forcing (Fig. 6) under the EQBO and WQBO conditions at lag 5–10 days of MJO P67, which corresponds to model time steps of 25–30 days. The LBM simulations reasonably well capture a PNA-like dipole pattern over the North Pacific region (Fig. 7a, b), although the negative center is exaggerated. A comparison of the two experiments reveals that the WQBO experiment has stronger MJO-teleconnection in the North Pacific than the EQBO experiment (Fig. 7c). In other words, a weaker MJO P67 forcing under the WQBO condition leads to stronger MJO teleconnections compared to a stronger forcing under the EQBO condition. This is consistent with the observation (Fig. 2e), supporting our hypothesis.

When imposing the MJO P34 and MJO P567 forcing separately in a model, it is evident that the EQBO-WQBO differences in the MJO P34 teleconnections are more pronounced than those in the MJO P567 teleconnections. The teleconnection pattern generated by MJO P34 forcing is out of phase with that generated by MJO P567 forcing (see Fig. 7d–f, g–i, respectively). As the contrast in MJO amplitude between EQBO and WQBO winters is greater in P34 than in P567, the lagged response of the MJO P34 teleconnections is more pronounced as compared to that of the MJO P567 teleconnections. This eventually leads to stronger MJO teleconnections under the WQBO condition than under the EQBO condition 5–10 days after the onset of MJO P67.

A parameter sweep experiment is carried out by changing W_{34}/E and W_{567}/E. Specifically, W_{34}/E is systematically varied from 0 to 1 with 0.2 increment, while W_{567}/E is varied from 0.4 to 1 with 0.1 increment. The MJO-teleconnection strength difference between the two QBO conditions is quantified with a dipole index (DIPO, hereafter). The DIPO is calculated by taking the average of 500-hPa geopotential height difference (EQBO-WQBO) in regions 1 and 2 as indicated in Fig. 7c, and then computing their differences (region 2 minus region 1). Positive value indicates stronger MJO-P67 teleconnections under the WQBO condition compared to the EQBO condition.

Figure 8 summarizes the experiment by displaying the DIPO index as a function of W_{34}/E and W_{567}/E. It shows a positive DIPO with decreasing W_{34}/E and/or increasing W_{567}/E (bottom right corner). Conversely, an increase in W_{34}/E and a decrease in W_{567}/E lead to a negative DIPO value. This result indicates that MJO-P67 teleconnections become stronger under the WQBO condition as MJO P567 is stronger (still weaker than the EQBO condition) and preceding MJO P34 is weaker.

The observed EQBO-WQBO difference (i.e., Fig. 7c) corresponds to W_{567}/E of 0.9 and W_{34}/E of 0.4 in Fig. 8 (box with a black border). However, if MJO P567 is significantly weakened while maintaining the MC-barrier modulation effect under the WQBO condition (e.g., $W_{34}/E = 0.4 < W_{567}/E = 0.6$), MJO teleconnections become weaker (e.g., DIPO = −2.89). Or, if there is no MC-barrier modulation effect while maintaining the amplitude modulation effect (e.g., $W_{34}/E = W_{567}/E = 0.8$), MJO teleconnections become weaker under the WQBO condition (e.g., DIPO = −2.28). This result suggests that much weaker MJO P34 without significant

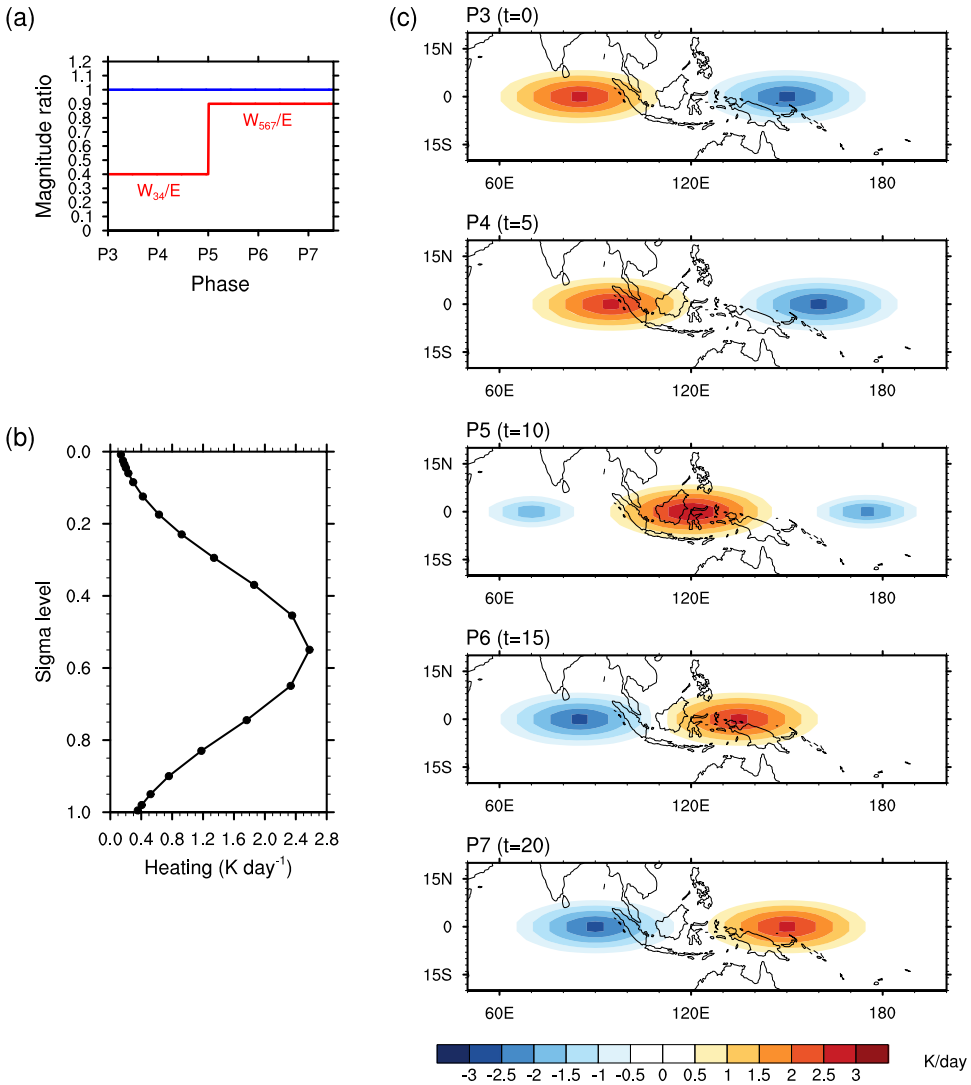

Fig. 6 The external forcing imposed in LBM. a Time series of the relative magnitude of forcing for the EQBO (blue) and WQBO experiments (red). Each MJO phase is set to persist for 5 days. **b** Vertical profile of the heating at the location of maximum heating (e.g., 85°E and 0° for MJO phase 3), and **c** horizontal distribution of the heating at $t = 0$, 5, 10, 15, 20, (t: model time steps) at 0.55 sigma level, mimicking the observed heating distribution at MJO phase 3, 4, 5, 6, 7, respectively. The horizontal heating distributions are linearly interpolated in time between consecutive MJO phases.

weakening of MJO P567 is required for stronger MJO teleconnections during the WQBO compared to the EQBO states.

DISCUSSION

This study investigates the strength and robustness of MJO teleconnections in the North Pacific during the EQBO and WQBO winters. It is found that MJO teleconnections are stronger and more robust at lag 5–10 days of MJO P67 during the WQBO winter than during the EQBO winter, although MJO amplitude is weaker during the former. By investigating the back trajectory of the MJO, we found that the majority of MJO P67 events during the WQBO winter are not preceded by active MJOs on the west of the MC (e.g., MJO P34) due to the QBO modulation of the MC-barrier effect. Since there is no opposing forcing prior to MJO P67, MJO P67 teleconnections could become stronger during the WQBO winter than during the EQBO winter. The linear model experiments support this conjecture. The simulated PNA-like MJO teleconnections in the North Pacific region are stronger for the WQBO condition compared to the EQBO condition when the preceding MJO amplitudes are much weaker than those of MJO P67. In terms of two competing effects of the QBO, i.e., the amplitude modulation effect (weaker MJO amplitude during the WQBO winter) and MC-barrier modulation effect (stronger MC barrier during the WQBO winter), the latter is critical for strong MJO-P67 teleconnections during the WQBO winter.

This result suggests that not only the MJO amplitude at a given time but also the MJO amplitude in the past should be taken into account to understand the MJO teleconnections in the North Pacific[39] where teleconnection impacts from both the current MJO phase and the preceding MJO phase have more tendency to coexist than other regions. This conclusion aligns with the argument of Zheng and Chang[40], emphasizing the importance of investigating the MJO lifecycle to comprehend its teleconnection patterns.

The MJO P23 is not influenced by the MC-barrier effect. Indeed, most MJO P23 events are traced back to P67 without any significant difference in the OLR anomalies between the two QBO phases (Supplementary Fig. 1). However, the MJO P23 teleconnections are not evidently stronger during the EQBO than WQBO winters. This is likely because the background-flow change does not facilitate MJO propagation into the North Pacific despite the

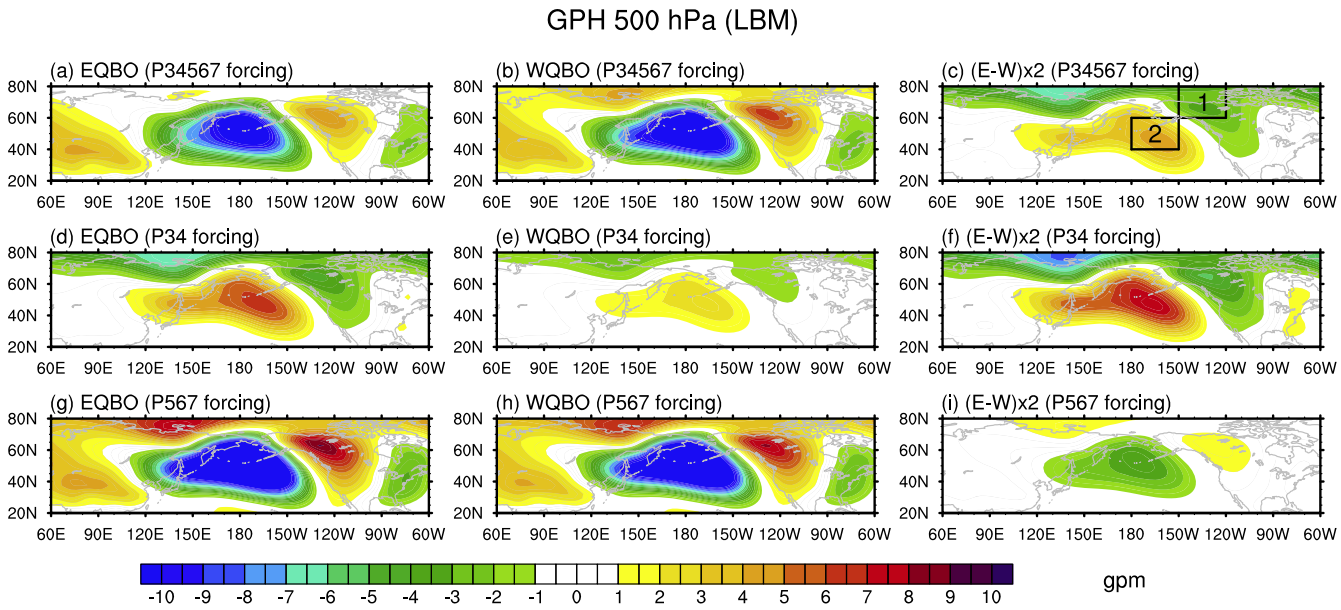

Fig. 7 Simulated teleconnections at lag 5–10 days of MJO P67 under the two QBO conditions. (Top) Linear responses of geopotential height at 500 hPa to the MJO forcing averaged for 5–10 days after the MJO P67 under the **a** EQBO (blue in Fig. 6a) and **b** WQBO conditions (red in Fig. 6a), and **c** the difference between the two experiments. (middle) **d**–**f** Same as in **a**–**c** but only the MJO P34 forcing is imposed. In this experiment, the forcing is maintained until P4 and then turned off after P5 in Fig. 6a. (bottom) **g**–**i** Same as in **a**–**c** but only the MJO P567 forcing is imposed. In this experiment, the forcing is turned on at P5 in Fig. 6a. Boxed regions 1 and 2 represent North America and the North Pacific regions, respectively. The region 2 average minus region 1 average is defined as the dipole index (DIPO).

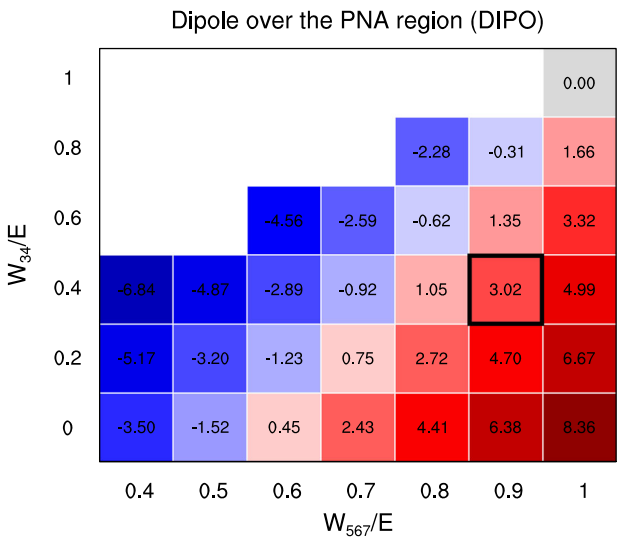

Fig. 8 Simulated dipole indices under varying W_{34}/E and W_{567}/E. Dipole index (DIPO) over the North Pacific region as a function of MJO amplitude ratio between WQBO experiment and EQBO experiment at phase 5–7 (W_{567}/E; *x* axis) and that between WQBO experiment and EQBO experiment at phase 3–4 (W_{34}/E; *y* axis). The positive value represents when the MJO-teleconnection in the North Pacific region is stronger under the WQBO condition than under the EQBO condition. The control experiment mimicking the composited EQBO and WQBO conditions (i.e., $W_{567}/E = 0.9$, $W_{34}/E = 0.4$) is denoted with a black border. Experiments with smaller W_{567}/E than W_{34}/E are masked, as they are less likely to occur.

stronger forcing during the EQBO winter. Although not statistically significant, the Asia-Pacific jet shifts poleward by the EQBO[22]. This background-flow change likely provides an unfavorable condition for the Rossby waves to propagate into the North Pacific. Therefore, the role of background flow needs to be considered in conjunction with understanding the back trajectory of the MJO.

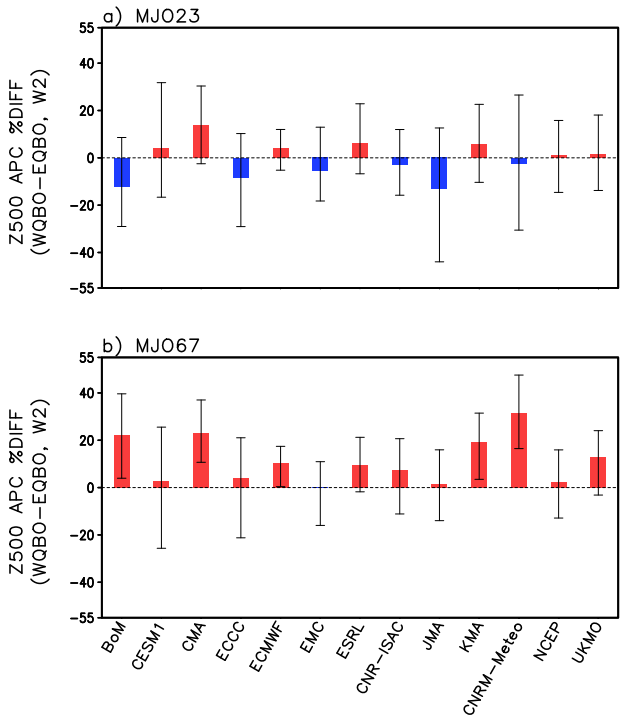

Fig. 9 WQBO–EQBO percent difference in 500-hPa geopotential height prediction skills. The percent difference in 500-hPa geopotential height prediction skill between **a** MJO P23 initializations during the WQBO winters and those during the EQBO winters in the North Pacific region (20°–70°N, 150°E–120°W) in the forecast week 2. **b** The same as **a** but for MJO P67 initializations. Prediction skill is quantified by using anomaly pattern correlation coefficient. Red colors represent higher prediction skills during the WQBO winters compared to the EQBO winters. The 95% confidence interval around the mean value is indicated by the error bar.

The QBO modulation of the strength and the robustness of MJO teleconnections can affect midlatitude prediction skill. Figure 9 shows the WQBO–EQBO percent difference in 500-hPa geopotential height prediction skills in the North Pacific at forecast week two. All available S2S predictions initialized at MJO P23 and P67 are utilized[41]. For MJO P67 initializations, all models show enhanced prediction skills during the WQBO winter than during the EQBO winter, with 7 out of 13 models showing statistically significant enhancement (Fig. 9b). Such systematic differences do not appear when the models are initialized at MJO P23 (Fig. 9a). This result suggests that enhanced MJO teleconnections during the WQBO winter can lead to improved midlatitude prediction skills in the North Pacific.

Several questions remain. Why is the MJO-teleconnection difference between the two QBO winters dependent on the MJO phase in the North Pacific, while showing no such dependency in the upstream (e.g., East Asia) or downstream regions (e.g., North Atlantic)? Intuitively, East Asia might have a more direct response to the MJO forcing[20], dominated by the lag 0 MJO amplitude modulation effect. On the other hand, the North Atlantic region as far downstream could be dominantly influenced by the propagation conditions of the Rossby waves. As the North Pacific region is situated between these two regions, it is likely affected by both MJO forcing and propagation conditions. Further investigations are necessary to understand the relative roles of MJO forcing and background state changes across these regions. Another remaining question lies in the underlying mechanisms by which the QBO affects the MJO trajectory, which also deserves future investigation.

This study aimed to understand the controversial QBO's impact on the MJO teleconnections in the North Pacific. The QBO modulation of MJO teleconnections is phase-dependent, with stronger and more robust MJO teleconnections during the WQBO winter only at phase 67. Very weak MJO convection in the west of the MC prior to MJO P67 likely causes such a difference despite a weaker MJO amplitude during the WQBO winter compared to the EQBO winter. This result not only helps us increase our understanding of the QBO modulation of the S2S prediction skill associated with MJO teleconnections but also gives us insights into a way to improve S2S prediction skill in the North Pacific by emphasizing the importance of MJO lifecycle in predicting MJO teleconnections.

METHODS

Reanalysis data and observations

ERA5 daily data[42], produced by the European Centre for Medium-Range Weather Forecasts (ECMWF), are employed at a spatial resolution of 1.5 by 1.5 degrees for 42-year period (1979–2020) to examine the MJO teleconnections. Geopotential height at 500-hPa pressure level is particularly used to diagnose the MJO teleconnections in the North Pacific, within the latitude range of 20°–70°N and the longitude range of 150°E to 120°W, following the approach of Tseng et al.[43]. NOAA OLR data[44] are utilized to analyze the convective activity associated with the MJO during the two different QBO phases. To isolate the MJO-related forcing and teleconnections, a Lanczos band-pass filter (20–100 days) is applied to geopotential height and OLR data. Results from using different band-pass filters (15–90 days or 30–60 days) are comparable to those obtained with the 20–100 day band-pass filter (Supplementary Fig. 2). Since the MJO-QBO connection is robust during the midwinter months, i.e., December–January–February (DJF)[13], we restrict our investigation to MJO events observed within these three months.

MJO and QBO indices

The OMI[45] is employed to define the MJO. Only cases with an OMI amplitude greater than or equal to 1 are considered as MJO events. When adjusting the OMI threshold to 0.7 or using Real-time Multivariate MJO (RMM) index, essentially the same conclusion is drawn (see Supplementary Fig. 2). Due to the limited sample size, all the analysis is carried out by combining two consecutive MJO phases (e.g., MJO P34). The EQBO and WQBO winters are defined when the DJF-mean 50-hPa zonal-mean zonal wind averaged over 10°N–10°S is >0.5 standard deviation and smaller than −0.5 standard deviation, respectively, of the DJF climatology. Only those years within the EQBO and WQBO periods characterized by neutral El Niño–Southern Oscillation (ENSO) conditions, defined by an Oceanic Niño index (ONI) amplitude less than 0.5, are selected. A complete list of EQBO and WQBO years, along with El Niño and La Niña years, is provided in Supplementary Table 1.

Analysis methods

Based on the MJO and QBO definitions, MJO phases are composited for EQBO and WQBO winters, respectively. While all MJO days are considered for the analysis, consecutive MJOs separated by other MJOs by more than seven days are treated as a single event when calculating the number of degrees of freedom[46]. To demonstrate Rossby wave propagation as evidence of the tropical-extratropical teleconnection, we calculated horizontal component of the stationary Rossby wave activity flux by Takaya and Nakamura[47]. Only wave activity flux statistically significant at the 95% confidence level is displayed. In addition to the composite analysis, the pattern consistency[31] is computed to quantify the robustness of the circulation anomalies induced by MJO teleconnections. The pattern consistency is calculated in the North Pacific region by first computing pattern correlation coefficient (PCC) between two arbitrary events out of all the events classified as certain MJO and QBO phases. After calculating the PCC from all the possible pair combinations at each phase and each time lag, the percentage of the pairs of which PCC exceeds a correlation of 0.5 is defined as the pattern consistency. Statistical significance is tested by performing a two-sampled t test. See Tseng et al.[31] for further details on the pattern consistency.

LBM

To validate the QBO modulation of MJO teleconnections in the observations, a set of experiments is conducted using LBM[48]. The LBM employs linearized hydrostatic primitive equations about a basic state and has served as a diagnostic tool for simulating the linear response to a prescribed forcing. A spectral resolution of the LBM is set to T42 with 20 sigma levels in the vertical. For the numerical damping, fourth-order biharmonic diffusion with a e-folding timescale of two hours is applied to the largest wavenumber. The 20-day damping timescale is used in each level except for the bottom three and top two levels having 0.5-day damping timescale.

S2S prediction

Long-term reforecasts of thirteen operational models, sourced from the S2S prediction project[49], the subseasonal experiment project (SubX[50]), and 46-level CESM1 model are also utilized to investigate the QBO modulation of the prediction skill of MJO teleconnections after MJO P23 and P67 in the North Pacific region. The thirteen models are BoM, CMA, CNR-ISAC, CNRM-Meteo, ECCC, ECMWF, JMA, KMA, UKMO, NCEP, 46LCESM1, EMC-GEFS, and ESRL-FIM. Detailed information on these models can be found in Kim et al.[41]. In the calculation of the prediction skill, anomaly pattern correlation coefficient[41,51] is used.

DATA AVAILABILITY

The ERA5 data[42] are accessible at https://cds.climate.copernicus.eu/cdsapp#!/home. OLR data[44] and OMI index[45] are downloaded from https://psl.noaa.gov/data/gridded/data.olrcdr.interp.html and https://psl.noaa.gov/mjo/mjoindex/, respectively.

CODE AVAILABILITY

The source code used to analyze this study is available from the first author upon reasonable request.

Received: 31 August 2023; Accepted: 1 January 2024;
Published online: 09 January 2024

REFERENCES

1. Madden, R. A. & Julian, P. R. Detection of a 40–50 day oscillation in the zonal wind in the tropical Pacific. *J. Atmos. Sci.* **28**, 702–708 (1971).
2. Madden, R. A. & Julian, P. R. Description of global-scale circulation cells in the tropics with a 40–50 day period. *J. Atmos. Sci.* **29**, 1109–1123 (1972).
3. Hoskins, B. J. & Karoly, D. J. The steady linear response of a spherical atmosphere to thermal and orographic forcing. *J. Atmos. Sci.* **38**, 1179–1196 (1981).
4. Seo, K. H. & Son, S. W. The global atmospheric circulation response to tropical diabatic heating associated with the Madden–Julian oscillation during northern winter. *J. Atmos. Sci.* **69**, 79–96 (2012).
5. Mori, M. & Watanabe, M. The growth and triggering mechanisms of the PNA: a MJO-PNA coherence. *J. Meteorol. Soc. Japan* **86**, 213–236 (2008).
6. Moore, R. W., Martius, O. & Spengler, T. The modulation of the subtropical and extratropical atmosphere in the Pacific basin in response to the Madden–Julian oscillation. *Mon. Weather Rev.* **138**, 2761–2779 (2010).
7. Yoo, C., Lee, S. & Feldstein, S. B. Mechanisms of Arctic surface air temperature change in response to the Madden–Julian oscillation. *J. Clim.* **25**, 5777–5790 (2012).
8. Seo, K. H. & Lee, H. J. Mechanisms for a PNA-like teleconnection pattern in response to the MJO. *J. Atmos. Sci.* **74**, 1767–1781 (2017).
9. Yoo, C. & Son, S. W. Modulation of the boreal wintertime Madden-Julian oscillation by the stratospheric quasi-biennial oscillation. *Geophys. Res. Lett.* **43**, 1392–1398 (2016).
10. Baldwin, M. P. et al. The quasi-biennial oscillation. *Rev. Geophys.* **39**, 179–229 (2001).
11. Anstey, J. A. et al. Impacts, processes and projections of the quasi-biennial oscillation. *Nat. Rev. Earth Environ.* **3**, 588–603 (2022).
12. Wang, F. & Wang, L. An exploration of the connection between quasi-biennial oscillation and Madden-Julian oscillation. *Environ. Res. Lett.* **16**, 114021 (2021).
13. Son, S. W., Lim, Y., Yoo, C., Hendon, H. H. & Kim, J. Stratospheric control of the Madden–Julian oscillation. *J. Clim.* **30**, 1909–1922 (2017).
14. Nishimoto, E. & Yoden, S. Influence of the stratospheric quasi-biennial oscillation on the Madden–Julian oscillation during austral summer. *J. Atmos. Sci.* **74**, 1105–1125 (2017).
15. Hendon, H. H. & Abhik, S. Differences in vertical structure of the Madden-Julian oscillation associated with the quasi-biennial oscillation. *Geophys. Res. Lett.* **45**, 4419–4428 (2018).
16. Zhang, C. & Zhang, B. QBO-MJO connection. *J. Geophys. Res. Atmos.* **123**, 2957–2967 (2018).
17. Martin, Z., Wang, S., Nie, J. & Sobel, A. The influence of the quasi-biennial oscillation on the Madden-Julian oscillation in idealized cloud-resolving simulations. *J. Geophys. Res. Atmos.* **76**, 669–688 (2019).
18. Sakaeda, N., Dias, J. & Kiladis, G. N. The unique characteristics and potential mechanisms of the MJO-QBO relationship. *J. Geophys. Res. Atmos.* **125**, e2020JD033196 (2020).
19. Martin, Z. et al. The influence of the quasi-biennial oscillation on the Madden–Julian oscillation. *Nat. Rev. Earth Environ.* **2**, 477–489 (2021).
20. Kim, H., Son, S. W. & Yoo, C. QBO modulation of the MJO-related precipitation in East Asia. *J. Geophys. Res. Atmos.* **125**, e2019JD031929 (2020).
21. Feng, P. N. & Lin, H. Modulation of the MJO-related teleconnections by the QBO. *J. Geophys. Res. Atmos.* **124**, 12022–12033 (2019).
22. Park, C. H., Son, S. W., Lim, Y. & Choi, J. Quasi-biennial oscillation-related surface air temperature change over the western North Pacific in late winter. *Int. J. Climatol.* **42**, 4351–4359 (2022).
23. Baldwin, M. P. & Dunkerton, T. J. Stratospheric harbingers of anomalous weather regimes. *Science* **294**, 581–584 (2001).
24. Song, L. & Wu, R. Modulation of the westerly and easterly quasi-biennial oscillation phases on the connection between the Madden–Julian oscillation and the Arctic Oscillation. *Atmosphere* **11**, 175 (2020).
25. Marshall, A. G., Hendon, H. H., Son, S. W. & Lim, Y. Impact of the quasi-biennial oscillation on predictability of the Madden–Julian oscillation. *Clim. Dyn.* **49**, 1365–1377 (2017).
26. Lim, Y., Son, S. W., Marshall, A. G., Hendon, H. H. & Seo, K. H. Influence of the QBO on MJO prediction skill in the subseasonal-to-seasonal prediction models. *Clim. Dyn.* **53**, 1681–1695 (2019).
27. Baggett, C. F., Barnes, E. A., Maloney, E. D. & Mundhenk, B. D. Advancing atmospheric river forecasts into subseasonal-to-seasonal time scales. *Geophys. Res. Lett.* **44**, 7528–7536 (2017).
28. Mundhenk, B. D., Barnes, E. A., Maloney, E. D. & Baggett, C. F. Skillful empirical subseasonal prediction of landfalling atmospheric river activity using the Madden–Julian oscillation and quasi-biennial oscillation. *npj Clim. Atmos.* **1**, 20177 (2018).
29. Jenney, A. M., Randall, D. A. & Barnes, E. A. Quantifying regional sensitivities to periodic events: application to the MJO. *J. Geophys. Res. Atmos.* **124**, 3671–3683 (2019).
30. Mayer, K. J. & Barnes, E. A. Subseasonal midlatitude prediction skill following quasi-biennial oscillation and Madden–Julian Oscillation activity. *Weather Clim. Dyn.* **1**, 247–259 (2020).
31. Tseng, K. C., Barnes, E. A. & Maloney, E. D. Prediction of the midlatitude response to strong Madden-Julian Oscillation events on S2S time scales. *Geophys. Res. Lett.* **45**, 463–470 (2018).
32. Hoskins, B. J. & Ambrizzi, T. Rossby wave propagation on a realistic longitudinally varying flow. *J. Atmos. Sci.* **50**, 1661–1671 (1993).
33. Garfinkel, C. I. & Hartmann, D. L. The influence of the quasi-biennial oscillation on the troposphere in winter in a hierarchy of models. Part I: simplified dry GCMs. *J. Atmos. Sci.* **68**, 1273–1289 (2011).
34. Simpson, I. R., Blackburn, M. & Haigh, J. D. The role of eddies in driving the tropospheric response to stratospheric heating perturbations. *J. Atmos. Sci.* **66**, 1347–1365 (2009).
35. Lin, H. & Brunet, G. Extratropical response to the MJO: nonlinearity and sensitivity to the initial state. *J. Atmos. Sci.* **75**, 219–234 (2018).
36. Garfinkel, C. I. & Hartmann, D. L. The influence of the quasi-biennial oscillation on the troposphere in winter in a hierarchy of models. Part II: perpetual winter WACCM runs. *J. Atmos. Sci.* **68**, 2026–2041 (2011).
37. Huang, K. & Pegion, K. The roles of westward-propagating waves and the QBO in limiting MJO propagation. *J. Clim.* **35**, 6031–6049 (2022).
38. Alaka, G. J. & Maloney, E. D. The influence of the MJO on upstream precursors to African easterly waves. *J. Clim.* **25**, 3219–3236 (2012).
39. Tseng, K. C., Maloney, E. & Barnes, E. The consistency of MJO teleconnection patterns: an explanation using linear Rossby wave theory. *J. Clim.* **32**, 531–548 (2019).
40. Zheng, C. & Chang, E. K. The role of MJO propagation, lifetime, and intensity on modulating the temporal evolution of the MJO extratropical response. *J. Geophys. Res. Atmos.* **124**, 5352–5378 (2019).
41. Kim, H., Son, S.-W., Kim, H., Seo, K.-H. & Kang, M.-J. MJO influence on subseasonal-to-seasonal prediction in the Northern Hemisphere extratropics. *J. Clim.* **36**, 7943–7956 (2023).
42. Hersbach, H. et al. The ERA5 global reanalysis. *Q. J. R. Meteorol. Soc.* **146**, 1999–2049 (2020).
43. Tseng, K. C., Maloney, E. & Barnes, E. A. The consistency of MJO teleconnection patterns on interannual time scales. *J. Clim.* **33**, 3471–3486 (2020).
44. Liebmann, B. & Smith, C. A. Description of a complete (interpolated) outgoing longwave radiation dataset. *Bull. Am. Meteorol. Soc.* **77**, 1275–1277 (1996).
45. Kiladis, G. N. et al. A comparison of OLR and circulation-based indices for tracking the MJO. *Mon. Weather Rev.* **142**, 1697–1715 (2014).
46. Garfinkel, C.I., Feldstein, S. B., Waugh, D. W., Yoo, C. & Lee, S. Observed connection between stratospheric sudden warmings and the Madden-Julian Oscillation. *Geophys. Res. Lett.* **39**, L18807 (2012).
47. Takaya, K. & Nakamura, H. A formulation of a phase-independent wave-activity flux for stationary and migratory quasigeostrophic eddies on a zonally varying basic flow. *J. Atmos. Sci.* **58**, 608–627 (2001).
48. Watanabe, M. & Kimoto, M. Atmosphere-ocean thermal coupling in the North Atlantic: a positive feedback. *Q. J. R. Meteorol. Soc.* **126**, 3343–3369 (2000).
49. Vitart, F. et al. The subseasonal to seasonal (S2S) prediction project database. *Bull. Am. Meteorol. Soc.* **98**, 163–173 (2017).
50. Pegion, K. et al. The Subseasonal Experiment (SubX): a multimodel subseasonal prediction experiment. *Bull. Am. Meteorol. Soc.* **100**, 2043–2060 (2019).
51. Dias, J. & Kiladis, G. N. The influence of tropical forecast errors on higher latitude predictions. *Geophys. Res. Lett.* **46**, 4450–4459 (2019).

ACKNOWLEDGEMENTS

This work was supported by the Korea Environment Industry &Technology Institute (KEITI) through "Climate Change R&D Project for New Climate Regime" funded by the Korea Ministry of Environment (MOE) (2022003560004), the National Research Foundation of Korea (NRF) grant funded by the Korea government (MSIT) (2023R1A2C3005607), and the NRF of Korea funded by the Ministry of Education (2021R1I1A1A01060303).

AUTHOR CONTRIBUTIONS

M.J.K., H.K., and S.W.S. conceptualized the study. M.J.K. and H.K. performed the analysis under the supervision of S.W.S. The manuscript was written by M.J.K., S.W.S., and H.K. All authors contributed to the interpretation and discussion of the results.

COMPETING INTERESTS

The authors declare no competing interests.

ADDITIONAL INFORMATION

Supplementary information The online version contains supplementary material available at https://doi.org/10.1038/s41612-024-00565-w.

Correspondence and requests for materials should be addressed to Seok-Woo Son.